2026 European Control Conference (ECC)
July 7-10, 2026. Reykjavík, Iceland

Multi-Modal LSTM-Based Tracking Control for a Soft Robotic Manipulator with Hysteresis

Benjamin D. Bassett[1], Afonso Dias[2], Jialei Shi[2], Fahim Shakib[3], Enrico Franco[2], and Kaiwen Chen[1]

Abstract— **This paper proposes a multi-modal control scheme for soft robotic manipulators with hysteretic elasticity, which allows tracking time-varying reference signals. Long Short-Term Memory (LSTM) networks are employed to estimate hysteresis moments in configurable frequency bands of the reference signal. For this purpose, supervisory training data is obtained by smoothing differentiated acceleration and solving a moment balance equation offline. Subsequently, a multi-modal control scheme is developed, which automatically selects, based on the reference spectrogram, the suitable LSTM estimator to track a variable-frequency reference signal. The proposed controller demonstrates superior tracking performance with respect to a baseline controller with integral action, for high-frequency reference signals, and to its single-modal version, for low-frequency references.**

I. INTRODUCTION

Compared to classical rigid-link robotic manipulators, soft robotic manipulators (SRMs) offer enhanced compliance, beneficial for interaction with delicate environments such as those found in surgery [1], semiconductor industry [2], and human-machine interaction [3]. Despite these advantages, the modelling and control of soft robots are challenging due to the inherent uncertainty and nonlinearity of the soft structure and the actuation mechanism (see, *e.g.*, [4], [5]). The majority of SRMs are made with hyper-elastic materials such as silicone rubber, offering high compliance with little to no permanent deformation. A popular choice for actuation of such SRMs is pneumatics, which offers high power-to-weight ratio and affordability [6]. These materials and actuation method, however, introduce hysteresis into the system. Hysteresis is a general term which refers to the dependence of a system's behavior on its time history [7]. Even at rest with no actuation force, the configuration of an SRM cannot be purely determined from the model if the time history is unknown. In particular, if the control task is to follow a time-varying trajectory, the induced hysteresis effects are also time-varying and cannot be effectively compensated for by classical controllers, like proportional-integral control, which are designed for constant disturbance rejection. This poses a significant challenge to high-precision control of SRMs.

This work has been partially supported by the Engineering and Physical Sciences Research Council (EPSRC) [grant number EP/X033546/1].

[1] B. D. Bassett and K. Chen are with the Department of Electronic and Electrical Engineering, Imperial College London, UK.

[2] A. Dias, J. Shi, and E. Franco are with the Department of Mechanical Engineering, Imperial College London, UK.

[3] F. Shakib is with the Department of Mechanical Engineering, Eindhoven University of Technology, The Netherlands.

E-mails: benjamindbassett@gmail.com, m.f.shakib@tue.nl, {a.dias24, j.shi, e.franco11, kaiwen.chen16}@imperial.ac.uk.

Models describing hysteresis generally fit into two categories: operator-based and differential-based. Operator-based models are simpler and rely on explicit knowledge of the time history. The simplest model, namely the Preisach Model [8], is a two-valued operator akin to a Schmitt Trigger. More complex models with non-binary operators use integral and summative operations to encode the time-history. One such model is the Prandtl-Ishlinskii model [9]. Differential-based models formulate an internal state and a corresponding update law to encode the time history. These models do not require an explicit knowledge of the time history. Two notable examples are the Duhem [10] and Bouc-Wen models [11]. Both operator-based and differential-based models consider only symmetrical hysteresis, which can be limiting in engineering practice.

While model-free control is a popular choice for fully-actuated SRMs, model-based control provides superior performance, stability guarantees, and a reduced computational load [12], [13]. Popular model-based approaches include inverse-dynamics control, which requires accurate knowledge of the system model [14]; sliding mode control (SMC), specifically, uses localized high-gain feedback to reject bounded uncertainties and disturbances [15]. This type of inverse dynamics control requires a model with minimal uncertainty - either derived from first principles [4] or from data through machine learning (ML) networks [16]. Alternatively, inverse-dynamics adaptive control and adaptive-observer integration methods require uncertainties and disturbances to be linearly parametrized, and might respond more slowly to the reference signal, depending on specific tuning [17]–[19]. However, hysteretic elasticity is not accurately represented by a bounded disturbance or by a constant unknown parameter. Consequently, new approaches are required to address this type of uncertainty.

Data-driven approaches represent a promising avenue for hysteresis compensation. In particular, the long short-term memory (LSTM) network is a type of recurrent neural network (RNN). This configuration lends itself to modelling of time-history dependent effects. Preliminary work indicates that LSTM networks can model hysteretic effects of an operator-based (Preisach) system [20]. LSTM networks have also been applied to adaptive control, showing the potential of combining data-driven and model-based methodologies into an integrated control design [21], [22]. Finally, LSTM have networks been employed to address model uncertainties [23] and to estimate unmeasured states [24].

The contribution of this work is an LSTM-based control scheme for time-varying reference tracking of a soft robotic manipulator. In particular, to improve the LSTM-based estimation, we adopted a multi-modal LSTM algorithm, in which each LSTM network is trained to estimate the unmeasurable hysteresis state within a certain frequency band of the reference signal. A classifier is utilized to detect frequency characteristics of the reference signal, so that the most suitable LSTM network can be activated accordingly to improve tracking performance. An inverse-dynamics controller with disturbance rejection modifications is employed as a baseline to guarantee a uniformly bounded tracking error with an adjustable ultimate bound. The effectiveness of this approach is demonstrated with experiments on an SRM prototype.

II. MODELLING AND SYSTEM IDENTIFICATION

The SRM and its model are the basis for the LSTM network and hysteresis identification methods constructed in later sections. We introduce the prototype immediately following.

A. Equipment Setup

1) Manipulator Prototype: The SRM prototype considered in this paper is made of a compliant silicone-based elastomer, initially designed for robotic colonoscopy. The manipulator is cylindrical and extensible, and it bends about a central axis. Internally, 9 reinforced chambers are partitioned uniformly along the perimeter of the cross-section and operated in 3 groups of 3 chambers. The cross-section layout is uniform along the central axis, see Fig. 1, with detailed dimensions reported in [25].

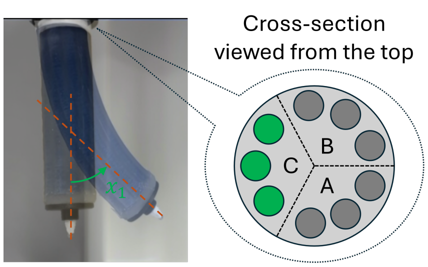

Fig. 1. Schematic of a bending SRM (green circles are the pressurized chambers that cause the bending action).

While a manipulator of such a structure can bend on any plane (see [18]), this paper only considers operation on a single plane. This is to emphasize the reference tracking of the tip-angle. The extension to a general bending plane is immediate as a consequence of modelling assumptions.

2) Actuation and Sensing: Digital pressure regulators with a maximum output of 3 bar are used to control the pressure in the trios of chambers independently. The angular position and attitude of the tip are recorded with an Electromagnetic (EM) sensor (NDI, Canada). This is converted into tip angle, x_1, and used to compute angular velocity, x_2. To robustify the process to noise, a high-pass filter is employed so that x_2 can be acquired in real time.

B. Manipulator Model

We introduce a common assumption for continuum robots to quantitatively describe the kinematics of the SRM.

Assumption 1 (Constant curvature and length): The length L of the manipulator is constant, and the shape of the manipulator is subject to a constant curvature (CC) constraint (see, *e.g.*, [4]). ⋄

Assumption 1 essentially states that the shape of the SRM can be determined by an arc of constant length, and the bending of the SRM can be described by the variation of the radius of the circle containing the arc. This allows describing the deformed shape of the SRM with a 1 degree-of-freedom (DoF) model. Since the SRM is actuated by a single bending moment due to internal pressurization, the underlying model is fully actuated. This assumption holds provided that the SRM has a constant section, its structure is homogeneous, and no external force is imposed on the system. Although this is an approximation, it is sufficiently accurate for the system considered in this work.

The generalized model of the one-segment SRM with a differential-based hysteresis effect is described by

$$\dot{x}_1 = x_2, \tag{1a}$$

$$M(x_1)\dot{x}_2 = -\left(C(x_1,x_2)+D\right)x_2 - G(x_1) - K(x_1) - z + \tau \tag{1b}$$

$$\dot{z} = f(z,x), \tag{1c}$$

where $z(t) \in \mathbb{R}$ denotes the hysteresis moment; $\tau(t) \in \mathbb{R}$ is the actuation moment generated by air pressure (the control input); $C\left(x_1(t),x_2(t)\right)x_2(t) \in \mathbb{R}$ represents the centrifugal and Coriolis moment; $M\left(x_1(t)\right) \in \mathbb{R}$ is the mass resulting from the material distribution that can be determined by Assumption 1, see [4]. The restorative moments, $K(x_1)$ and $G(x_1)$, and the damping coefficient $D > 0$ can be experimentally identified. We denote the quantities that are identified or approximated by $\hat{(\cdot)}$ from their ground-truth counterparts $(\cdot)$. The function $f(z,x)$, with $x \triangleq [x_1,x_2]^\top$, describes the evolution of z in a differential-based hysteresis model. In this paper, we do not exploit the analytical form of $f(z,x)$ but, instead, estimate z from experimental data.

C. Experimental Identification

The damping coefficient and restorative moments are identified per the SRM prototype.

1) Damping Coefficient: The identification of the linear damping coefficient is done by manually exciting the manipulator and recording the time histories of the bending angle. The envelope of the bending angle response is constructed from the Hilbert transform of the time series. The damping coefficient corresponding to the convergence rate is estimated by taking the linear fitting of the semi-log plot of the envelope, which yields $D = 1.9 \times 10^{-5}$ Nms/rad.

2) Restorative Moments: Both the stiffness and gravitation moments are restorative and are present when the system is at rest in any state aside from the zero state (*i.e.*, the SRM is straight and without deformation). We leverage this property to identify a restorative moment mapping. To eliminate dynamic effects, the actuation pressure is increased in small steps of 5 mbar, and it is maintained until the SRM reaches steady-state. Both an ascending and a descending phase are recorded. The static mapping is identified by linear least-squares fitting, see Fig. 2. We define the restorative moment $R(\cdot):\mathbb{R}\to\mathbb{R}$ as $G(x_1)+K(x_1)$, which can be approximated by the piecewise function

$$\begin{aligned}\hat{R}(x_1) &= \hat{G}(x_1)+\hat{K}(x_1)\\ &= \begin{cases} a_5x_1^5+a_4x_1^4+a_3x_1^3+a_2x_1^2+a_1x_1+c, & x_1\le 0,\\ b_5x_1^5+b_4x_1^4+b_3x_1^3+b_2x_1^2+b_1x_1+c, & x_1>0,\end{cases}\end{aligned} \tag{2}$$

with constant parameters $a_1,a_2,a_3,a_4,a_5,b_1,b_2,b_3,b_4,b_5$, and c. Two different polynomials are needed because the static mapping does not have two-fold rotational symmetry.

D. Hysteretic Moment

The deviation between the mean and the loop-shape trajectory in Fig. 2 is due to hysteresis. The hysteresis effect can be described by a moment depending on the time history of the SRM, or equivalently, approximated by a dynamically updated internal state as seen in (1c). The hysteresis loop is not 2-fold rotationally symmetric, a common characteristic of generalized hysteresis models. We therefore map the hysteresis moment in the following section using the LSTM networks.

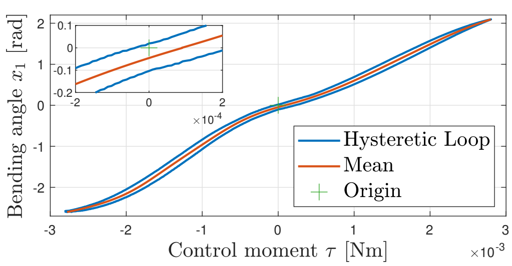

Fig. 2. Bending angle versus actuation moment (hysteresis loop).

III. LSTM-Based Estimator

The purpose of leveraging LSTM networks is to estimate the hysteresis moment based on the bending angle, angular velocity measurements, and control input. We build a reduced-order observer for z from experimental data, without requiring an accurate analytical expression of (1c). This allows relaxing the limitations of, for example, symmetry of the internal hysteresis dynamics. This section details the architecture and the training procedure of the LSTM network.

A. Basic Configuration

An LSTM cell has an internal state which motivates an asymmetrical approximation of a differential-based hysteresis model. We design a simple architecture to target specific frequency bands of the reference signal. It is necessary to have an efficient construction so that it does not add significant latency when used for negative-feedback control action; we enforce this by using a single LSTM layer, as opposed to the commonly used stacked LSTM (SLSTM) [21]. The resultant network consists of: 1) A sequence input layer. 2) An LSTM layer with multiple LSTM cells. 3) A fully connected output layer. The LSTM layer is configured and trained with the settings shown in Table I. Training settings were tuned iteratively: epochs were raised until the error metric could no longer decrease, and hidden units were selected to capture nonlinearity while reducing over-fitting. The training practice showed that only a few hidden units (≤ 10) are necessary to model the estimator for the hysteresis state, while using more units can generate unreliable estimation.

TABLE I
Hyperparameters of LSTM Training

Network Configuration	
Features (input)	$X_1=(x_{1,k}:k\in K)$ and $X_2=(x_{2,k}:k\in K)$ where K is the index set of time-history data points collected
Responses (output)	$\hat{z}$
Response Scaling	$10^4\times$
Hidden Units	5
Training	
Solver	Adaptive Moment Estimation (ADAM)
Epochs	5000

B. Training Data for Supervised Learning

The LSTM training is conducted with the actuation input set to step- and sine-type signals with randomized (and variable) frequency within a pre-selected range. The amplitude is randomized, and the sine reference signals are continuous. The step-type actuation signals are of the form:

$$\tau(t)=\gamma A_0(t_k),\quad \text{for } t\in[t_k,t_{k+1}), \tag{3}$$

where $A_0(t_k)$ is a time-sequence randomly generated from a uniform distribution over $[-2,2]$ and γ is the scalar conversion from pressure (bar) to torque. At each sampling instant t_k, A_0 is updated by a newly generated value with a probability 0.05. Once A_0 is updated, there is a 3-second dwell period before a new update can be performed. The sine actuation signals are of the form:

$$\tau(t)=\gamma A_1(t_k)\sin\left(2\pi\omega(t_k)t\right),\quad \text{for } t\in[t_k,t_{k+1}), \tag{4}$$

where $A_1(t_k)$ and $\omega(t_k)$ are time-sequences randomly generated from the uniform distributions over $[-2,2]$ and $[0.1,\ 0.167]$, respectively. Both A_1 and ω are updated once the current sine wave completes half of its period.

Different from classical LSTM training, the learning target z cannot be directly acquired from the experiment data since it is not measured. A straightforward fix to this is to solve (1b) for z, with the acceleration signal $\dot{x}_2$ approximated *post facto* by filtered differentiation using a moving average window (length: 10 samples), to attenuate noise amplified across sequential differentiations. Rearranging (1b), we employ the following equation to reconstruct the z signal

$$z^*=\tau-\hat{M}(x_1)\hat{\dot{x}}_2-\hat{C}(x_1,x_2)x_2-\hat{D}x_2-\hat{R}(x_1), \tag{5}$$

where $\hat{\dot{x}}_2$, denotes the non-causal approximation of the angular acceleration and z^* denotes the reconstructed signal. The z^*

sequences are normalized to allow for a more granular training process.

IV. CONTROLLER DESIGN

The control task considered in this paper is for the bending angle $x_1(t)$ to track a time-varying reference signal $r_1(t)$. The following assumptions are required for control synthesis.

Assumption 2: Let $r_2 \triangleq \dot{r}_1$ and $r_3 \triangleq \ddot{r}_1$. Then, r_1, r_2, and r_3 are known and essentially bounded. $\diamond$

Assumption 3: The hysteresis subsystem (1c) is bounded-input bounded-state stable with respect to the input x. $\diamond$

Assumption 4: The estimation errors for $C(x_1,x_2)$, D, $R(x_1)$, and $z(t)$ are bounded for all $|e| \leq \delta_e$ and $t \geq 0$, where δ_e is an user-specified parameter. $\diamond$

Assumption 5: The estimate of the inertia matrix satisfies $|M(x_1)\hat{M}(x_1)^{-1} - I| < \frac{1}{2}$, for all $|e| \leq \delta_e$ and $t \geq 0$. $\diamond$

A. Baseline Control

To guarantee tracking performance in the presence of uncertainties, we include a "baseline" controller that enforces an ultimate bound of the tracking error $e = [x_1 - r_1,\, x_2 - r_2]^\top \triangleq [e_1, e_2]^\top$. To this end, consider a classical "inverse-dynamics"-type control law

$$a = -k^\top e + r_3 + \eta, \tag{6a}$$

$$\tau = \hat{M}(x_1)a + \hat{C}(x_1,x_2)x_2 + \hat{D}x_2 + \hat{R}(x_1) + \hat{z}, \tag{6b}$$

where τ, a, and η are the actuation moment (control input), the desired acceleration, and the compensation term to attenuate the effects of uncertainties, respectively; $k \triangleq [k_P, k_D]^\top$ with $k_P > 0$, $k_D > 0$ the P, D gains, respectively; $\hat{(\cdot)}$ denotes the estimate (either from identification or generated by LSTM) of the true quantity $(\cdot)$. Define $A \triangleq \begin{bmatrix} 0 & 1 \\ -k_P & -k_D \end{bmatrix}$, $B \triangleq \begin{bmatrix} 0 \\ 1 \end{bmatrix}$. The compensation term η is generated by the system described as follows.

$$\dot{\xi} = \operatorname*{proj}_{\rho_1}(\xi, k_I s) \triangleq \begin{cases} 0, & \xi \leq -\rho_1 \text{ and } k_I s \leq 0, \\ 0, & \xi \geq \rho_1 \text{ and } k_I s \geq 0, \\ k_I s, & \text{otherwise}, \end{cases} \tag{7a}$$

$$\kappa = \rho_2 \frac{s}{\max(|s|, \varepsilon)}, \tag{7b}$$

$$\eta = -\xi - \kappa, \tag{7c}$$

where $P = P^\top \succ 0$ is the solution of the Lyapunov equation $A^\top P + PA + Q = 0$, for some $Q = Q^\top \succ 0$; $s \triangleq B^\top Pe$ is a passive signal for high-gain feedback, computed from the measurement; ρ_1, ρ_2, and k_I are positive tuning parameters.

The compensation term η contains both the integral action and the localized high-gain feedback because, in practical tracking scenarios in which the reference signal is varying around a constant value, the resulting state-dependent uncertainty will have an "averaged" constant component and a time-varying component. This allows us to exploit the *congelation of variables* method [26] to separately compensate the constant component using the integral action ξ (effective for slow-varying uncertainties) and dominate the time-varying perturbation using the localized high-gain feedback κ (more responsive to fast uncertainties) [27]. The controller achieves the closed-loop properties stated by the next theorem, for which the detailed proof is omitted due to limited space.

Theorem 1: Under Assumptions 1–5, consider the system (1) and the baseline controller (6) and (7). Then, for any initial tracking error $|e(0)| \leq \delta_{e_0}$, with a user-specified δ_{e_0}, and any selection of positive k_P and k_D, there exist positive constants k_I, ε, ρ_1, and ρ_2 such that: 1) all closed-loop signals are uniformly bounded; 2) e converges to a uniform ultimate bound adjustable via k_I and ε; and 3) if the model knowledge is perfect, $\lim_{t\to\infty} e(t) = 0$. $\diamond$

B. Multi-Modal Control

Despite the baseline control providing a worst-case performance guarantee, the LSTM networks are essential to improve control performance. Experiments show that using a single LSTM network for both set-point regulation and time-varying reference tracking does not achieve the best possible performance (see Section V). In light of this, we develop two LSTM-based estimators. Each estimator is trained with data that covers a preassigned, separate frequency range. A classification threshold w_l is then selected to differentiate high frequency references from largely static trajectories with occasionally transient "jumps", that is

- $\omega < \omega_l$: low-frequency LSTM Observer - trained using random step references.
- $\omega \geq \omega_l$: high-frequency LSTM Observer - trained using random sine references.

To automatically switch to the most suitable LSTM model from the trained LSTMs, according to the reference signal (which is correlated to the hysteresis moment at steady state), a classifier based on short-time Fourier transform (STFT) is applied to the reference input. This method is applied "offline" since the reference signal is known a priori and the window can be non-causal[1]. This allows acquiring the dominant frequency of the signal centred at each sample.

During implementation, a moving window of 201 samples (8 s at a sampling rate approximately 25 Hz) is applied to the reference signal and its average across the window is removed, and the remaining sequences are zero-padded to achieve a resolution of 1×10^4. Fig. 3 depicts a demonstration of the classification mechanism on a reference signal and the associated STFT spectrum plot.

V. EXPERIMENTAL RESULTS

In all the experiments discussed in this section, we consider the following baseline control settings: $k_p = 1 \times 10^3$, $k_d = 1$, $\rho_1 = 1 \times 10^3$, $\rho_2 = 1$, $s = e_2 + 100e_1$, and k_i is the main tuning parameter to be specified later. We refer to the control scheme using the baseline controller only as the "baseline" scheme, the baseline controller with the LSTM network trained from step actuation signals as the "low-ω" scheme, the baseline controller with the LSTM network trained from sinusoidal

[1]If implemented in real time, the window must be causal and the classification will be delayed depending on the window length, in which case the trade-off between the frequency resolution and classification time needs to be considered.

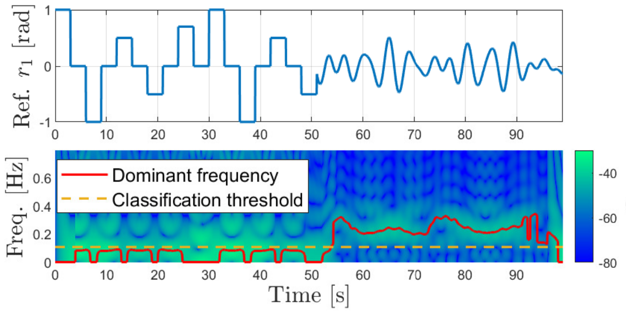

Fig. 3. Dominant frequency extraction of repeated reference signal for LSTM-control scheme classification.

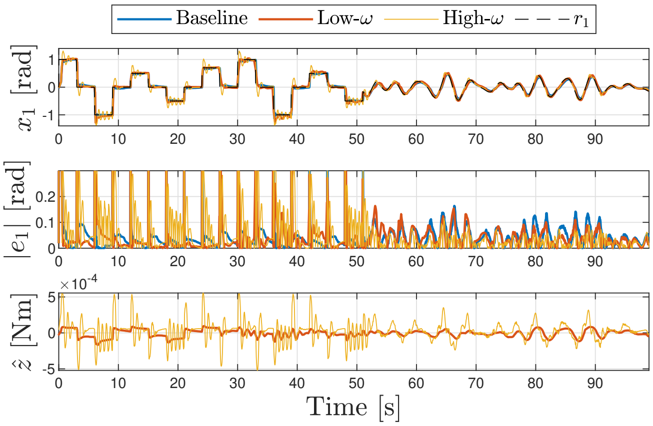

Fig. 4. Time histories of SRM controlled by single-modal controllers with the setting $k_i = 4$.

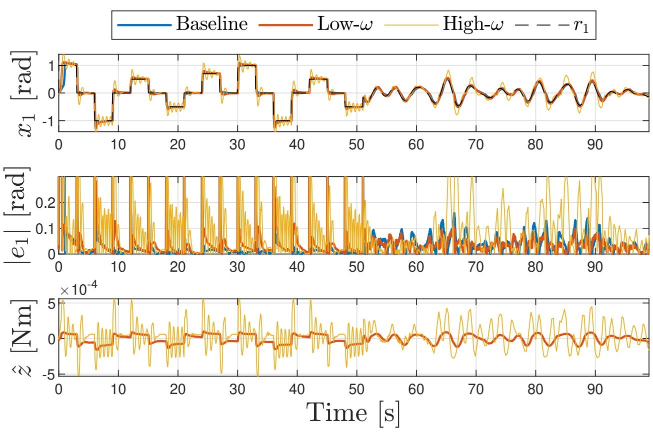

Fig. 5. Time histories of SRM controlled by single-modal controllers with the setting $k_i = 10$.

actuation signals as the "high-ω" scheme, and the baseline controller with the classifier and the switching LSTM network models as the "multi-modal" scheme.

A. Single-Modal Control

We first examine the performance of single-modal control schemes, under two different settings of $k_i = 4$ and $k_i = 10$, respectively. The experimental results are shown in Figs. 4 and 5, and the corresponding root-mean squared error (RMSE) are summarized in Tables II and III.

The RMSE errors indicate that, although increasing the integral gain allows the baseline control to achieve better compensation for the time-varying hysteresis effect and therefore track the sine (high-frequency) reference better, its tracking performance for step (low-frequency) signals degrades. This is consistent with the "waterbed" effect, according to which the sensitivity function cannot be lowered at all frequencies. This also explains why classical PID control of hysteretic systems is mostly tuned for set-point regulation, as further accounting for time-varying trajectory tracking will sacrifice the transient performance for set-point tracking. In contrast, the low-ω scheme performs better at both low and high frequencies. This is because the LSTM network compensates for the hysteresis effect more promptly than the classical integral action, which avoids the error accumulation in the integral control and therefore achieves better transient performance. The high-ω scheme tracks the high-frequency references best for the lower integral control gain. It, however, worsens the tracking performance for the step reference signals, and even the sine tracking performance is degraded when the integral gain is increased. Such a phenomenon is caused by the oscillatory behaviour of the high-ω LSTM network that enables tracking of non-constant signals.

These observations motivate a multi-modal control scheme utilizing each LSTM model in its specialized frequency band, and with a relatively lower integral gain.

B. Multi-Modal Control

The same reference trajectory is used to test the multi-modal control scheme (with $k_i = 4$). The classifier defined in Section IV-B with $w_l = 0.11$ Hz is employed to switch between the low-ω and high-ω LSTMs. The experimental results is shown in Fig. 6 and the RMSEs is summarized in the last column of Table II. In comparison with the two settings of the baseline control, the RMSE of the proposed multi-modal scheme is reduced by 46.1% and 40.8%, respectively, for time-varying reference tracking, which verifies the advantage of the proposed scheme in time-varying reference tracking over the classical method. It also maintains a comparable performance over the piecewise constant set-point tracking, which avoids the performance degradation of the single-modal controller with a high-ω LSTM network.

TABLE II
TRACKING RMSEs WITH $k_i = 4$

Ref.	Baseline	Low-ω	High-ω	Multi-mod.
Step	1.500×10^{-1}	1.498×10^{-1}	1.794×10^{-1}	1.509×10^{-1}
Sine	6.33×10^{-2}	5.40×10^{-2}	3.91×10^{-2}	3.41×10^{-2}
All	1.148×10^{-1}	1.133×10^{-1}	1.310×10^{-1}	1.094×10^{-1}

VI. CONCLUSIONS

In this paper, a multi-modal LSTM-based control scheme has been proposed to cope with the uncertainty due to the hysteresis effect inherent in soft robotic manipulators. Observer-like LSTM networks have been developed to estimate the

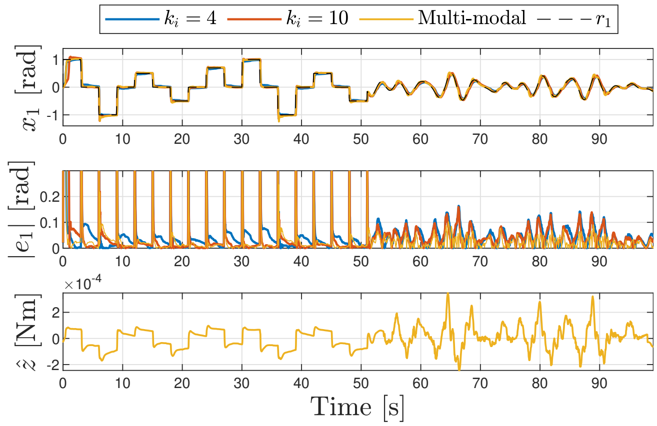

Fig. 6. Time histories of SRM controlled by the baseline controller with the settings $k_i = 4$ and $k_i = 10$, and by the multi-modal controller with the setting $k_i = 4$.

TABLE III

Tracking RMSEs with $k_i = 10$

Ref.	**Baseline**	**Low-ω**	**High-ω**
Step	1.658×10^{-1}	1.486×10^{-1}	2.054×10^{-1}
Sine	5.76×10^{-2}	4.56×10^{-2}	1.365×10^{-1}
All	1.239×10^{-1}	1.099×10^{-1}	1.704×10^{-1}

unmeasured hysteresis moment, with each of them specialized in a certain frequency range. A baseline controller that combines integral control and localized high-gain feedback has been used to guarantee the ultimate boundedness of the tracking error. Experiments have demonstrated that the proposed multi-modal scheme outperforms both the baseline controller and all single-modal approaches for time-varying reference tracking.

Future work will focus on the development of the switching logic when more than two models are involved, and will investigate the trade-offs between training time, LSTM network complexity, and the bandwidth of the reference signals that can be tracked with specified performance. Experiments will also be generalized to include a second DoF.

References

[1] M. S. Runciman, A. Darzi, and G. P. Mylonas, "Soft robotics in minimally invasive surgery," *Soft Robot.*, vol. 6, pp. 423 – 443, 2019.

[2] M. Akar, B. Mura, and Y. Oniz, "Design and manufacture of a low-cost soft gripper for industrial applications," in *2025 7th Int. Congr. Human-Comput. Interaction, Optim. and Robotic Appl. (ICHORA)*, 2025, pp. 1–6.

[3] S. B. Goyal, A. S. Rajawat, and A. K. J. Al-Nussairi, "Advanced soft robotics in healthcare: Enhancing patient assistance with machine learning, soft actuators, and human-robot interaction algorithms," in *2024 Int. Conf. Augmented Reality, Intell. Syst., and Ind. Automat. (ARIIA)*, 2024, pp. 1–7.

[4] C. Della Santina, C. Duriez, and D. Rus, "Model-based control of soft robots: A survey of the state of the art and open challenges," *IEEE Control Syst. Mag.*, vol. 43, no. 3, pp. 30–65, 2023.

[5] D. C. Rucker and R. J. Webster, "Mechanics-based modeling of bending and torsion in active cannulas," in *2008 2nd IEEE RAS & EMBS Int. Conf. Biomed. Robot. and Biomechatron.*, 2008, pp. 704–709.

[6] E. Franco and A. Garriga-Casanovas, "Energy Shaping Control of Soft Continuum Manipulators with in-plane Disturbances," *The Int. J. Robot. Res.*, vol. 40, no. 1, pp. 236–255, 2021.

[7] J. A. Ewing, "On the production of transient electric currents in iron and steel conductors by twisting them when magnetised, or by magnetising them when twisted," *Proc. Roy. Soc. London*, vol. 36, pp. 117–135, 1883.

[8] F. Preisach, "Über die magnetische Nachwirkung," *Zeitschrift für Physik*, vol. 94, no. 5, pp. 277–302, May 1935.

[9] M. Al Janaideh, S. Rakheja, and C.-Y. Su, "An analytical generalized Prandtl–Ishlinskii model inversion for hysteresis compensation in micropositioning control," *IEEE/ASME Trans. Mechatronics*, vol. 16, no. 4, pp. 734–744, 2011.

[10] P. M. M. Duhem, *Sur Les Déformations Permanentes et l'hysteresis.* Bruxelles: Hayez, 1896.

[11] Y.-K. Wen, "Method for random vibration of hysteretic systems," *J. Eng. Mechanics Division*, vol. 102, no. 2, pp. 249–263, 1976.

[12] A. AlAttar, I. B. Hmida, F. Renda, and P. Kormushev, "Kinematic-model-free tip position control of reconfigurable and growing soft continuum robots," in *2023 IEEE Int. Conf. Soft Robot. (RoboSoft)*, 2023, pp. 1–7.

[13] S. Treratanakulchai, E. Franco, and F. Rodriguez y Baena, "Model-free position control of a soft continuum manipulator in Cartesian space," in *2023 Int. Conf. Control, Automat. and Diagnosis (ICCAD)*, 2023, pp. 1–6.

[14] M. Armoon, M. Lafouti, B. Tavassoli, and H. D. Taghirad, "Robust inverse dynamics control of the remotely operated underwater vehicle manipulator," in *2022 8th Int. Conf. Control, Instrum. and Automat. (ICCIA)*, 2022, pp. 1–6.

[15] W. Zhu, M. Cheng, Y. Lang, and Q. Ren, "Variable stiffness control of a soft rehabilitation robot with sliding mode method," in *2023 35th Chin. Control and Decis. Conf. (CCDC)*, 2023, pp. 1514–1519.

[16] A. Garriga-Casanovas, F. Shakib, V. Ferrandy, and E. Franco, "Hybrid control of soft robotic manipulator," *Actuators*, vol. 13, no. 242, 2024.

[17] L. Wang, K. Chen, and E. Franco, "Robust and adaptive control of a soft continuum manipulator for minimally invasive surgery," *Robotics*, vol. 13, no. 11, p. 162, 2024.

[18] E. Franco, A. Garriga-Casanovas, J. Tang, F. Rodriguez y Baena, and A. Astolfi, "Adaptive energy shaping control of a class of nonlinear soft continuum manipulators," *IEEE ASME Trans. Mechatron.*, vol. 27, no. 1, pp. 280–291, 2022.

[19] E. Franco, T. Ayatullah, A. Sugiharto, A. Garriga-Casanovas, and V. Virdyawan, "Nonlinear energy-based control of soft continuum pneumatic manipulators," *Nonlinear Dyn.*, vol. 106, no. 1, pp. 229–253, 2021.

[20] W. Raczka, M. Sibielak, and J. Konieczny, "Modelling hysteresis with neural network," *2023 24th Int. Carpathian Control Conf. (ICCC)*, pp. 394–399, 2023.

[21] X. Shen, E. J. Griffis, W. Wu, and W. E. Dixon, "Adaptive control via Lyapunov-based deep long short-term memory networks," *IEEE Trans. Autom. Control*, vol. 70, no. 9, pp. 6199–6205, 2025.

[22] R. G. Hart, E. J. Griffis, O. S. Patil, and W. E. Dixon, "Lyapunov-based physics-informed long short-term memory (LSTM) neural network-based adaptive control," *IEEE Control Syst. Lett.*, vol. 8, pp. 13–18, 2024.

[23] E. J. Griffis, O. S. Patil, Z. I. Bell, and W. E. Dixon, "Lyapunov-based long short-term memory (Lb-LSTM) neural network-based control," *IEEE Control Syst. Lett.*, vol. 7, pp. 2976–2981, 2023.

[24] E. J. Griffis, O. S. Patil, R. G. Hart, and W. E. Dixon, "Lyapunov-based long short-term memory (Lb-LSTM) neural network-based adaptive observer," *IEEE Control Syst. Lett.*, vol. 8, pp. 97–102, 2024.

[25] J. Shi, K. Borvorntanajanya, K. Chen, E. Franco, and F. R. y. Baena, "Design, control, and evaluation of a novel soft everting robot for colonoscopy," *IEEE Trans. Robot.*, vol. 41, pp. 4843–4859, 2025.

[26] K. Chen and A. Astolfi, "Adaptive control for systems with time-varying parameters," *IEEE Trans. Autom. Control*, vol. 66, no. 5, pp. 1986–2001, 2021.

[27] K. Chen and A. Astolfi, "On the adaptive tracking problem of time-varying systems using the congelation for variables method," *IFAC-PapersOnLine*, vol. 56, no. 1, pp. 13–18, 2023.